Amplification of the storm surges in shallow waters of the Pertuis Charentais (Bay of Biscay, France)

Amandine Nicolle · Mikhail Karpytchev · Michel Benoit

Abstract The Pertuis Charentais are shallow coastal embayments formed by the islands of Oleron and Re in the north-eastern Bay of Biscay. The low-lying coasts of the Pertuis Charentais are susceptible to extensive flooding caused by the storm surges generated in the North Atlantic. Numerical modelling of the 24 October 1999 surge event is performed in the present study in order to elucidate the impact of the wind-wave-tide-surge interactions on the surge propagation in the Pertuis Charentais. A 2D numerical model is constructed to simulate the wave and tide-surge propagation on a high-resolution finite-element grid by using the TELEMAC and TOMAWAC software. The effect of the wave-induced enhancement on the sea surface drag and on the bottom friction is evaluated by using the models of Janssen (1991) and Christoffersen and Jonsson (1985), respectively. The radiation stress is estimated by employing the approach of Longuet-Higgins and Stewart (1964). It is demonstrated that the peak surge in the night on 23–24 October has been amplified inside the Pertuis Charentais by about 20 cm due to the wind-wave inter- actions with the tide-surge currents. These interactions are strongest at the entrance to the Pertuis Charentais where the sea surface drag coefficient is significantly increased by the wind-wave coupling. The effect of the wave-tide-surge interactions is large enough to be included in the flood forecasting systems of this region.

Keywords Storm surge · Tide · Wave · Wind · Pertuis Charentais · Numerical modelling

A. Nicolle
IFREMER, DYNECO/PHYSED,
Plouzané, France

M. Karpytchev (✉)
LIENSs CNRS UMR 6250, Université de La Rochelle,
2 rue Olympe de Gouges,
17000 La Rochelle, France
e-mail: mikhail.karpytchev@univ-lr.fr

M. Benoit
Saint-Venant Laboratory for Hydraulics,
Université Paris Est (Joint Research Unit EDF R&D, CETMEF,
Ecole des Ponts ParisTech),
Chatou, France

1 Introduction

Accurate prediction of storm surge elevations is a problem of great importance in the coastal oceanography that represents a major concern of flood warning systems. The conventional tide–surge models developed in the past (Heaps 1965; Flather 2000) are based upon two-dimensional vertically integrated hydrodynamic equations being forced, along with the tidal forces, by atmospheric pressure gradients and wind traction related to wind speed by an empirical formula (e.g. Heaps 1965; Smith and Banke 1975), while the bottom friction is parameterised by a quadratic bottom stress with a time-independent drag coefficient (Proudman 1953). These models result, in many cases, in general agreement between observed and modelled surges, providing that the 2D approximation is relevant for the studied area (Carretero Albiach et al. 2000; Bernier and Thompson 2007). Nevertheless, neglecting the interactions between wind, tide–surge currents and waves can lead to systematic underestimation of the surge peak heights as well as to errors in the peak timing (Wolf et al. 1988; Jones and Davies 1998; Mastenbroek et al. 1993; Benoit et al. 1997; Xie et al. 2003; Wolf 2009). It has been found, for example, that the widely used empirical Smith and Banke formula

results in underestimation of the surge amplitude (Williams and Flather 2000; Mastenbroek et al. 1993). The impact of wave–current interactions on the surge dynamics can be weak or strong depending on storm type, wind direction, tidal currents, wave spectrum, water depth, sea bed roughness and coastal line geometry. Generally, the wave–current interactions are more pronounced in shallow waters where the waves are shoaling and the surface drag can be significantly enhanced (Brown and Wolf 2009) affecting, by this reason, the offshore surge propagation in the near-shore area (Davies and Lawrence 1995; Luettich et al. 1992).

This paper investigates the effect of wind–wave–current interactions on the surge propagation in the shallow embayments of the Pertuis Charentais (Fig. 1) situated in the northeastern part of Bay of Biscay, in France. The offshore storm surges entering the Pertuis Charentais are often accompanied by appreciable swell waves whose significant height exceeds 5 m (Idier et al. 2006). This observation suggests that the non-linear interactions between wind, waves, tide and surge can be enhanced in shallow waters of the Pertuis Charentais. To trace the impact of these interactions on surge dynamics is the purpose of the present study. Understanding the factors controlling the surges in the region is also a subject of practical importance because the extensive wetting and drying mud flats in the inner part of the Pertuis Charentais are a site of oyster aquaculture industry sensitive to flooding provoked by the passage of storm surges.

The paper is organised as follows. Section 2 describes the main hydrographical features of the Pertuis Charentais. Section 3 details the numerical models of the surge–tide and of the wave propagation. In Section 4, we present numerical simulations of the storm surge occurring during the night of 23–24 October 1999 that has been chosen as a typical surge in the region accompanied by high offshore swell waves. Section 5 discusses the results of numerical experiments and draws the conclusions.

2 The Pertuis Charentais: observations

2.1 Geographical setting

The Pertuis Charentais are located along the French Atlantic coast in the northeastern part of the Bay of Biscay. They represent two coastal embayments of approximately 30 by 15 km (Fig. 1). They are composed of the Pertuis Breton which is a passage between the island of Re and the continent and the Pertuis d'Antioche which is that between islands of Oleron and Re. The Pertuis Charentais are deeper in the west, near the seaward boundary where the water depth is about 30 m. The bottom shoals rapidly eastwards where a typical water depth is about 5 m. The inner eastern part of the Pertuis Charentais is bordered by extensive low-lying mud plains. Two principal rivers bringing fresh water in the sea of Pertuis are: the Charente with mean winter outflow of 76 m^3/s and the Seudre (1 m^3/s). Another much

Fig. 1 Bathymetric map of the Pertuis Charentais showing tidal stations (*circles*)
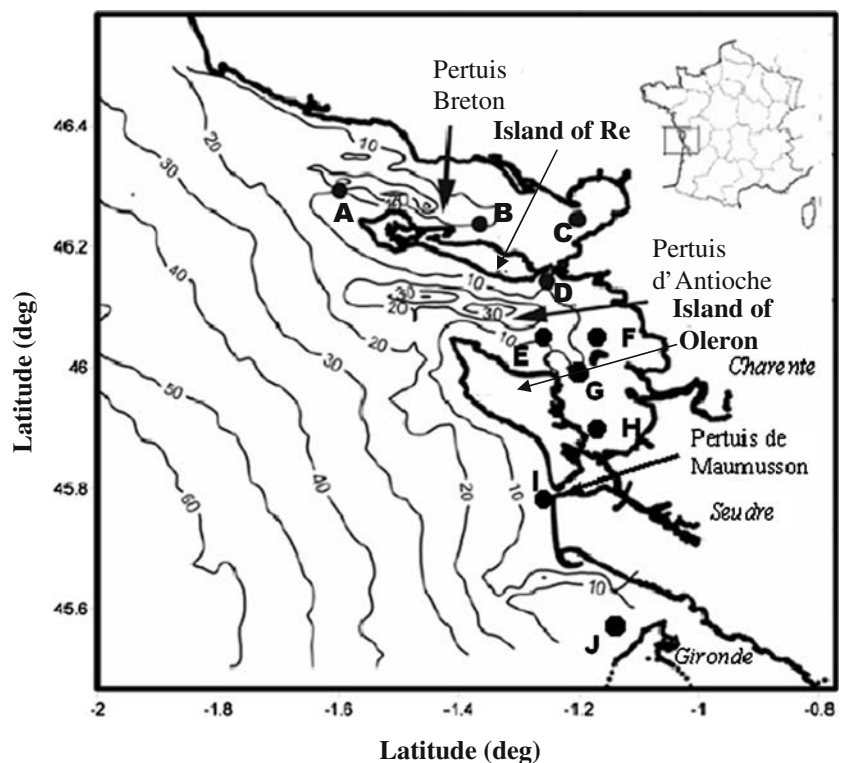
stronger river is the Gironde with a mean winter discharge of 1,440 m³/s. Although its discharge is important, the influence of the Gironde on the hydrodynamics in the Pertuis Charentais is usually negligible. It does not exclude, however, a pronounced impact of the Gironde River contaminants on the composition of the Pertuis Charentais water column.

2.2 Hydrodynamics

The circulation in the Pertuis Charentais, as in the whole Bay of Biscay, is dominated by the M2 semi-diurnal tide with a spring tidal range rising up to 6 m that corresponds to a macro-tidal region. To date, sea level measurements at ten stations are available for constraining a tidal model of the Pertuis Charentais (Fig. 1), two of them being permanent tidal stations: La Pallice (D in Fig. 1) and Le Verdon (J in Fig. 1). The observed amplitudes and phases of principal tidal constituents in the Pertuis are summarised in Table 1.

Unfortunately, during the October 1999 surge event, only tide gauge records from La Pallice (D in Fig. 1) and Chapus (H in Fig. 1) were available. These two tide gauges are located in areas of different seabed morphology and hydrodynamics: the La Pallice station is in the passage between the Pertuis Breton and the Pertuis d'Antioche which is covered mostly by sand dunes while the Chapus gauge is placed in a channel inside a shallow mud flat area wetting and drying for several kilometres during the spring tides.

3 The numerical models

3.1 Tides

The sea of Pertuis Charentais is shallow and well mixed, and the tidal elevations can be accurately evaluated from a barotropic model based on the depth-averaged shallow-water equations (Proudman 1953; Hervouet 2007):

$$\frac{\partial \eta}{\partial t} + \nabla(H\mathbf{u}) = 0 \tag{1}$$

$$\frac{\partial \mathbf{u}}{\partial t} + \mathbf{u}\nabla\mathbf{u} + \mathbf{f} \times \mathbf{u} = -g\nabla\eta + v\Delta\mathbf{u} + \mathbf{S_p} + \mathbf{S_w} + \mathbf{S_b} + \mathbf{S_{rad}} \tag{2}$$

where $\mathbf{u}=(u, v)$ is the depth-averaged horizontal velocity, η is the sea surface elevation, H is the total water depth, $\mathbf{f}$ is the upward pointing unit vector scaled by the Coriolis

Table 1 Observed amplitudes and phases of main tidal constituents in the Pertuis Charentais

Onde	A = Baleineaux Amplitude (m)	Phase (deg)	B = Saint Martin de Ré Amplitude (m)	Phase (deg)	C = Aiguillon Amplitude (m)	Phase (deg)	D = La Pallice Amplitude (m)	Phase (deg)	E = Balise Amplitude (m)	Phase (deg)	F = Ile d'Aix Amplitude (m)	Phase (deg)	G = Fort Boyard Amplitude (m)	Phase (deg)	H = Chapus Amplitude (m)	Phase (deg)	I = Gatseau Amplitude (m)	Phase (deg)	J = Verdon Amplitude (m)	Phase (deg)
O1	0.07	344	0.07	345	0.08	346	0.07	345	0.08	341	0.08	343	0.08	322	0.07	342	0.08	354	0.07	337
K1	0.07	99	0.07	99	0.07	100	0.07	100	0.08	90	0.06	86	0.06	68	0.06	101	0.07	100	0.06	87
N2	0.36	108	0.36	110	0.39	112	0.37	110	0.37	109	0.33	107	0.37	74	0.39	114	0.31	115	0.31	80
M2	1.60	128	1.75	131	1.81	133	1.76	131	1.72	128	1.79	127	1.78	94	1.68	131	1.47	133	1.54	130
S2	0.54	155	0.58	157	0.60	159	0.58	157	0.53	161	0.74	160	0.64	128	0.58	165	0.49	165	0.51	153
M4	0.18	70	0.27	74	0.29	79	0.27	74	0.23	68	0.25	69	0.27	1	0.23	83	0.14	55	0.08	81
M6	0.02	60	0.04	57	0.05	62	0.04	48	0.04	33	0.03	33	0.03	316	0.02	57	0.02	66	0.02	70

parameter, g is the gravity acceleration and ν is the eddy viscosity held constant in this study: $\nu=0.1$ m²/s (Bowden et al. 1974; Ezer and Mellor 2000). The vectors $\mathbf{S_p}$, $\mathbf{S_w}$, $\mathbf{S_b}$ ($\mathbf{S_b}=-(1/H\rho)\mathbf{\tau_b}$) and $\mathbf{S_{rad}}$ correspond to the atmospheric pressure at sea level, wind traction, bottom friction and the radiation stresses. The expressions for these forcing terms are detailed below. The bottom stress, $\mathbf{\tau_b}$, is formulated in the form of the Chezy law with a spatially variable friction coefficient (Nicolle and Karpytchev 2007).

Equations 1 and 2 have been solved by the TELEMAC-2D code (Hervouet and Van Haren 1994; Hervouet 2007) on a finite-element grid shown in Fig. 2. The grid domain (Fig. 2) comprises the Pertuis Charentais and the Gironde River and extends sufficiently far seaward to minimise the lack of precision in the tidal forcing at the open boundary. The entire grid consists of 6,373 triangular elements of variable size with a 5-km resolution near the seaward open boundary and about 100 m near the coast. The sea level and the tidal currents predicted on this grid by a tide-only model differ from those computed on a denser grid (up to 10^4 elements) by no more than 0.1%.

The tide-only model has been forced by specifying at the offshore open boundary the elevations of the following ten tidal constituents: SA, O1, K1, M2, S2, N2, K2, L2, NU2 and M4 which were obtained from the Bay of Biscay tidal model developed by the French Navy Hydrographical Service (Le Roy and Simon 2003). The accuracy of the

tidal model predictions is illustrated in Table 2: the mean difference between observations and predictions for the M2 amplitude is 2 and 0.8 cm for the M4 amplitude. More details about the tidal model can be found in Nicolle and Karpytchev (2007).

3.2 Surges

Surges have been computed as the difference between the water surface elevations driven by the sea level prescribed at the open boundary together with the meteorological forcing (wind stress and surface pressure) and those predicted by tide-only model. The numerical simulations have been performed by running the TELEMAC 2D through adding to the right-hand side of Eq. 2 a forcing term $\mathbf{S_p}$ due to the atmospheric pressure P_a and that due to wind, $\mathbf{S_w}$:

$$\mathbf{S_p} = -\frac{1}{\rho}\mathrm{grad}\,(P_a) \qquad (3)$$

where ρ=density of water

$$S_w = \frac{1}{H\rho}\mathbf{\tau}_s \qquad (4)$$

where H is the total water depth and $\mathbf{\tau_s}$ is the surface stress vector defined by the formula:$\tau_s = \rho_a \times C_d \times |U_{wind}|U_{wind}$ with ρ_a=1.023 kg/m³ is air density, U_{wind} the wind speed at 10 m and C_d the drag coefficient estimated either by the

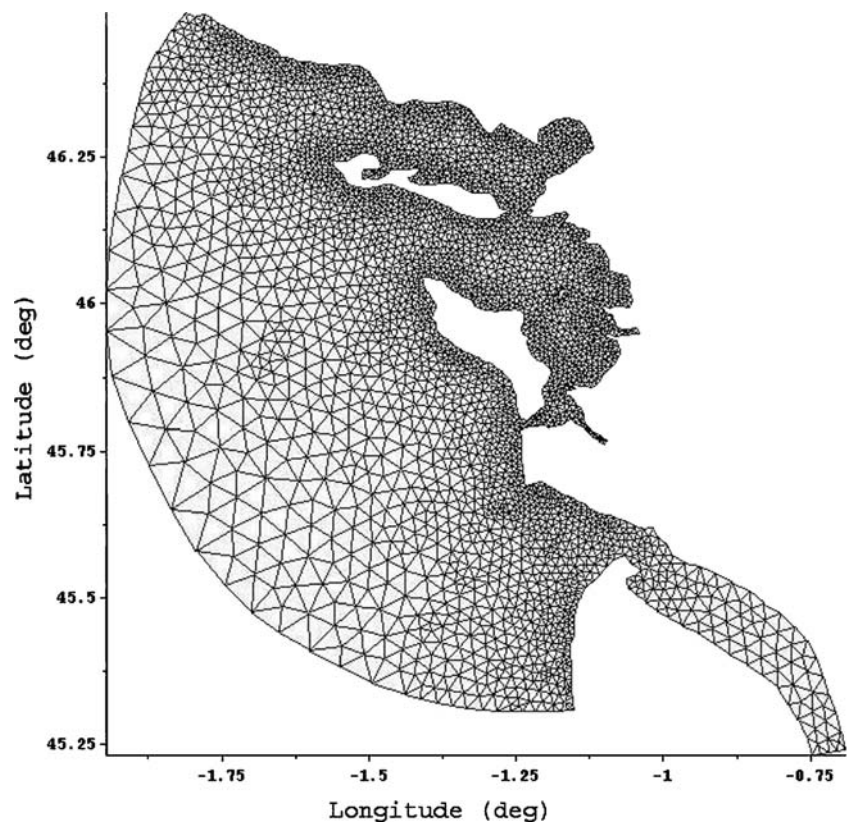Fig. 2 The finite-element grid used in the local model

Table 2 Predicted amplitudes and phases of main tidal constituents in the Pertuis Charentais

Onde	A = Baleineaux Amplitude (m)	Phase (deg)	B = Saint Martin de Ré Amplitude (m)	Phase (deg)	C = Aiguillon Amplitude (m)	Phase (deg)	D = La Pallice Amplitude (m)	Phase (deg)	E = Balise Amplitude (m)	Phase (deg)	F = Ile d'Aix Amplitude (m)	Phase (deg)	G = Fort Boyard Amplitude (m)	Phase (deg)	H = Chapus Amplitude (m)	Phase (deg)	I = Gatseau Amplitude (m)	Phase (deg)	J = Verdon Amplitude (m)	Phase (deg)
O1	0.08	354	0.08	355	0.08	357	0.08	356	0.08	355	0.08	358	0.08	355	0.08	359	0.08	4	0.08	350
K1	0.07	87	0.07	88	0.08	88	0.07	88	0.08	83	0.07	85	0.07	87	0.07	105	0.07	94	0.07	92
N2	0.30	104	0.33	106	0.36	109	0.35	107	0.35	106	0.31	104	0.33	104	0.37	110	0.29	111	0.29	76
M2	1.59	132	1.84	140	1.88	141	1.86	140	1.82	137	1.86	139	1.89	143	1.71	140	1.46	137	1.48	144
S2	0.50	147	0.56	150	0.58	153	0.57	151	0.56	157	0.58	150	0.59	154	0.54	160	0.44	151	0.44	153
M4	0.14	72	0.28	92	0.31	98	0.30	94	0.23	97	0.25	107	0.25	109	0.26	90	0.1	81	0.07	90
M6	0.01	35	0.04	31	0.06	38	0.06	52	0.03	35	0.02	33	0.02	34	0.03	63	0.02	52	0.02	63

method of Janssen (1991) presented briefly below or by the empirical formula of Smith and Banke (1975):

$$\begin{cases} C_d = 0.565 \cdot 10^{-3} & \text{if } U_{wind} < 5\text{m/s} \\ C_d = (-0.12 + 0.137 U_{wind}) \cdot 10^{-3} & \text{if } 5 < U_{wind} < 19.22\text{m/s} \\ C_d = 2.512 \cdot 10^{-3} & \text{if } U_{wind} > 19.22\text{m/s} \end{cases} \quad (5)$$

The wind velocity fields were provided by the meteorological model of NOAA-CIRES Climate Diagnostics Centre (USA; http://www.cdc.noaa.gov/cgi-bin/db_search/SearchMenus.pl). The spatial resolution of this model is 1°, and the wind fields are available every 6 h.

The combined tide–surge calculations take into account the non-linear interactions between tide and surge wave. In addition to the forcing terms S_p and S_w, the open-boundary forcing should be modified by adding the time-varying amplitude of the external surge generated outside the local model. At a given time, t, the sea level at the open boundary, ξ, is then a sum of amplitudes of the ten tidal constituents mentioned above and the amplitude of the offshore surge, S:

$$\xi(t) = S(t) + \sum_{i=1}^{n} a_i \cos(\omega_i t - \phi_i) \quad (6)$$

where a_i, ω_i, ϕ_i are the amplitudes, frequencies and phases of ten tidal constituents.

The offshore surge amplitudes specified in Eq. 6 along the open boundary are those predicted by the storm surge model on the European shelf (Fig. 3) developed by the Laboratoire National Hydraulique et Environnement of EDF (Electricité De France; Benoit et al. 1996). Note that the sea depth along the open boundary in Fig. 2 is about 50–60 m that makes the surge–tide interaction much less effective than in shallower waters and the superposition of surge and tide sea level elevations in Eq. 6 is likely to be justified.

3.3 Waves

The wave state in the Pertuis Charentais has been calculated by using the TOMAWAC model (Benoit et al. 1997; Benoit 2003) that estimates the time evolution of the directional spectrum F by solving the energy balance equation for waves:

$$\frac{\partial (B \cdot \widetilde{F})}{\partial t} + C_x \frac{\partial (B \cdot \widetilde{F})}{\partial x} + C_y \frac{\partial (B \cdot \widetilde{F})}{\partial y} + C_\theta \frac{\partial (B \cdot \widetilde{F})}{\partial \theta} + C_{fr} \frac{\partial (B \cdot \widetilde{F})}{\partial f_r} = B \cdot Q \quad (7)$$

where: $F(f, \theta) = \frac{Cg}{Cg + \overrightarrow{U} \cdot \overrightarrow{k}/k} \widetilde{F}(f_r, \theta)$ and $B = C \cdot Cg/(8\pi f_r^2)$
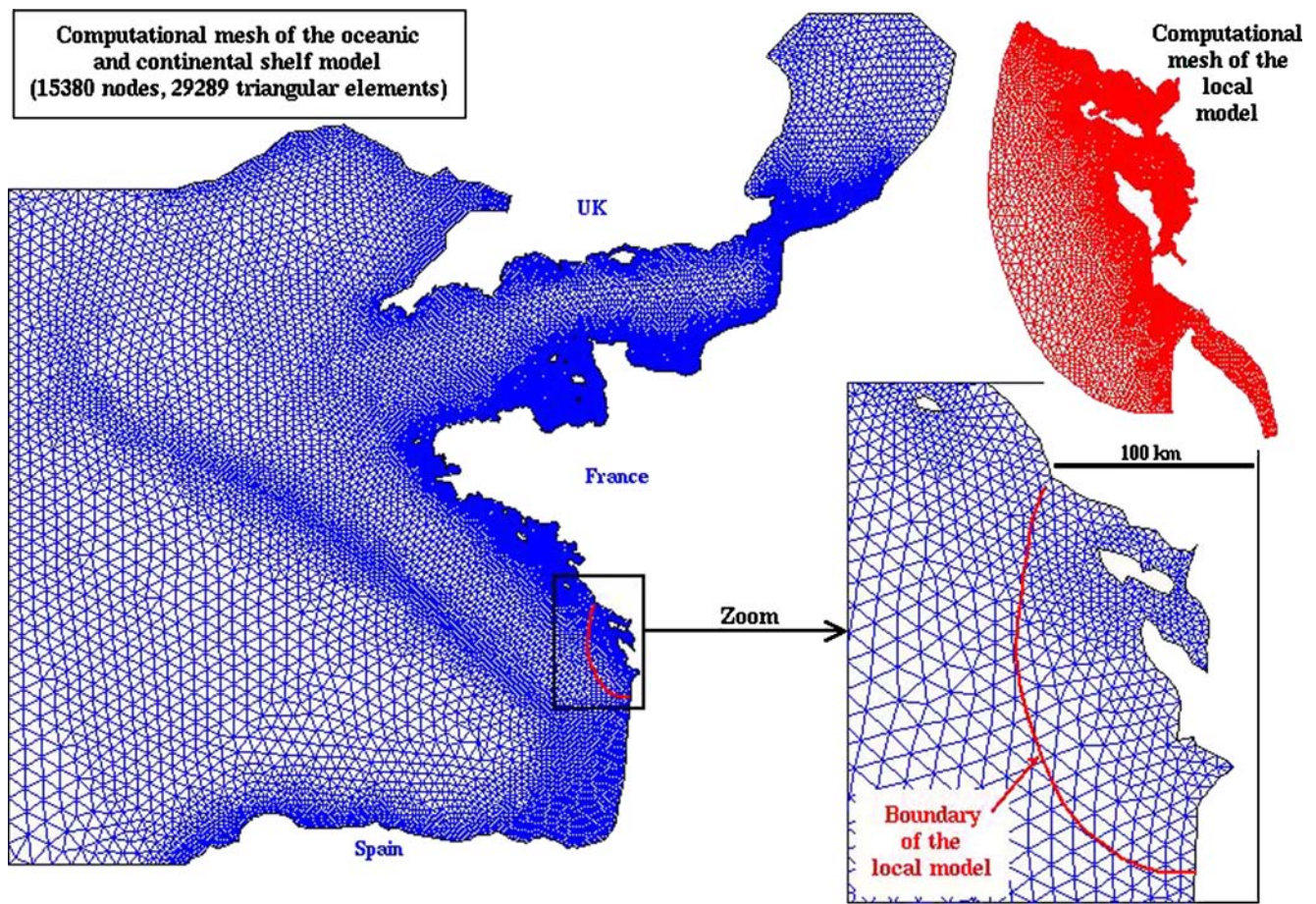
Fig. 3 The grid used by the continental shelf model of LNHE

Here, C and C_g are the phase and group velocities of waves. The directional wave spectrum $F(x, y, f_r, \theta, t)$ is a function of time t and spatial coordinates x and y as well as of the direction of propagation θ and relative frequency f_r of a wave component. The term Q stands for a sum of source terms representing the wave generation by wind, non-linear quadruplet interactions and the dissipative processes due to bottom friction, whitecapping and depth-induced breaking. The details about the parameterisation of these terms can be found in Benoit et al. (1996) and Benoit (2003).

Similar to the tide–surge model above, the wave in the local model (Fig. 2) has been driven by the wind and by prescribing at the open boundary the three-hourly wave spectrum computed by the wave propagation model around Europe (Fig. 3; Benoit et al. 1996). The spectrum predicted by the large-scale model was close to the JONSWAP shape (JONSWAP 1973). For this reason, we have parameterised the wave spectrum at the open boundary as a JONSWAP spectrum whose parameters (significant wave height, peak frequency) as well as the wave direction have been provided by the large-scale wave model.

3.4 The interactions between wind, waves, tide and surge

3.4.1 Surface stress

As indicated in Section 3.2, the formulation of surface stress used in TELEMAC 2D is based, by default, only on the wind speed. The independence of the surface stress of sea state is not realistic because the surface stress is rather sensitive to the sea surface roughness which is linked in its turn to wave characteristics. To take into account the interactions at the sea surface between the wind, waves and tide–surges, we have applied Janssen (1991) theory which is briefly presented below. The surface stress is considered as a sum of a turbulent stress τ_t and a wave stress τ_w:

$$\tau_s = \tau_w + \tau_t \tag{8}$$

The turbulent stress is obtained by applying the mixing length hypothesis:

$$\tau_t = \rho_a (\kappa \cdot z)^2 \left(\frac{\partial V}{\partial z}\right)^2 \tag{9}$$

Fig. 4 The computational scheme
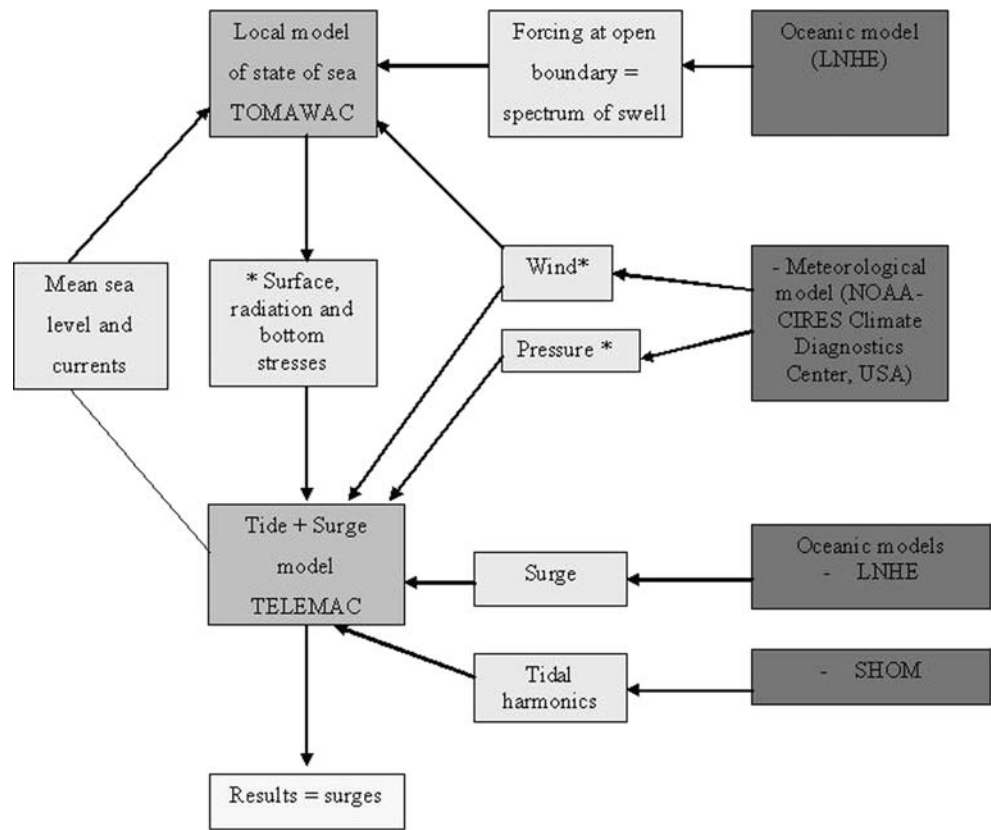
*: values are defined on the entire grid.

where κ is the Von Karman constant and $V(z)$ the wind speed. The vertical profile of wind is supposed to follow a logarithmic law:

$$V(z) = \frac{u_*}{\kappa} \ln\left(\frac{z + z_e - z_0}{z_e}\right) \qquad (10)$$

where $u_* = \sqrt{\tau_s/\rho_a}$ is the friction velocity; z_0 and z_e are, respectively, the roughness lengths in the absence and presence of waves. The effective roughness can then be expressed as:

$$z_e = \frac{z_0}{\sqrt{1 - \tau_w/\tau_s}} \qquad (11)$$

Fig. 5 The wind speed and direction (dashed line) on 23–25 October 1999
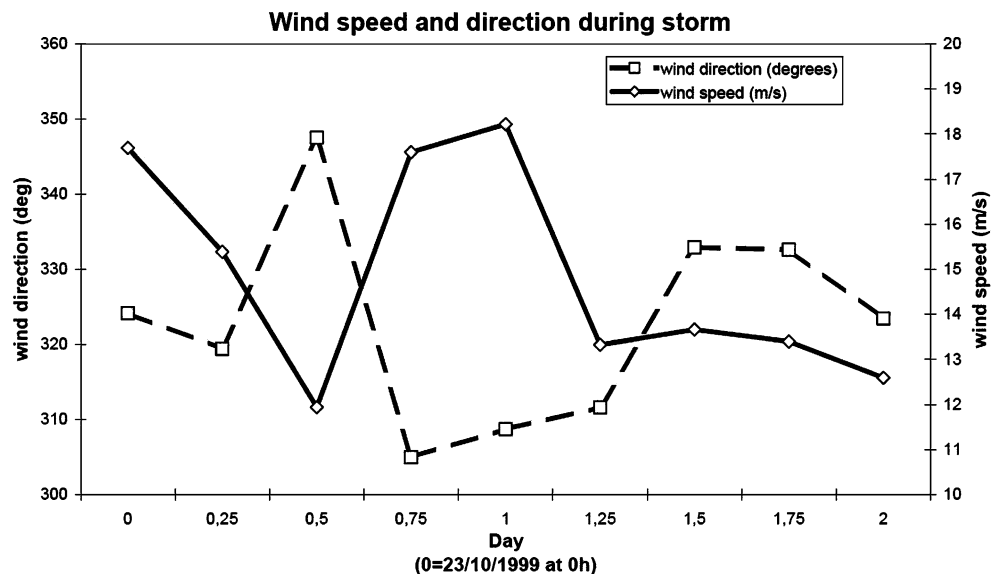
Fig. 6 Observed surge on 23–24 October 1999 at La Pallice (*solid line*) and Chapus (*dashed line*)
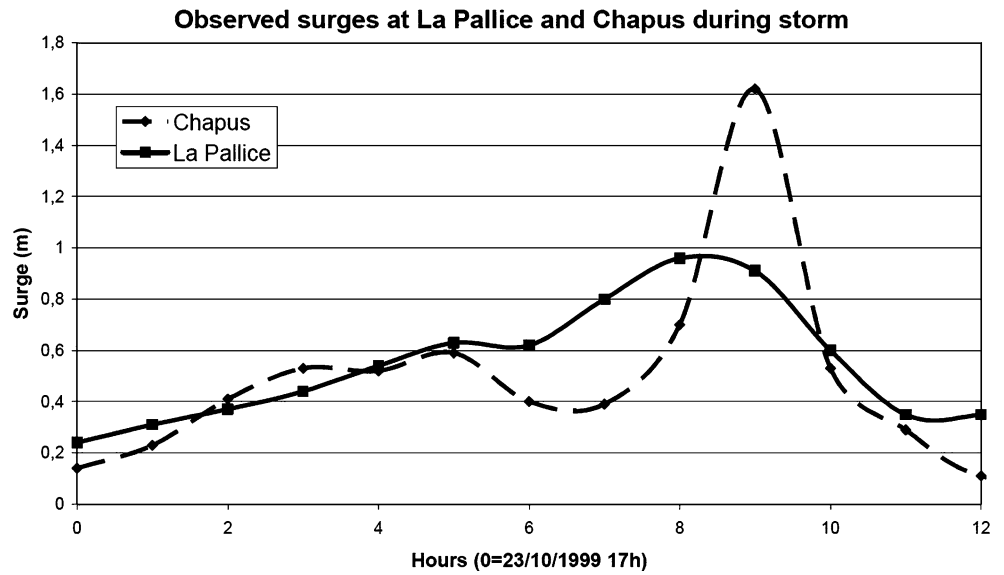
where z_0 is obtained from the classical Charnock relationship. Taking into account the wave-induced stress, τ_w, computed by TOMAWAC in wave propagation model, an iteration procedure similar to that of Mastenbroek et al. (1993) has been used to estimate z_0, z_e and τ_s.

3.4.2 Bottom stress

Another important type of interaction between waves and tidal–surge currents in shallow waters occurs due to intensifying of bottom turbulence by waves. The orbital

Fig. 7 The hindcast of the significant wave height (m) at 22:00 h on 23 October 1999
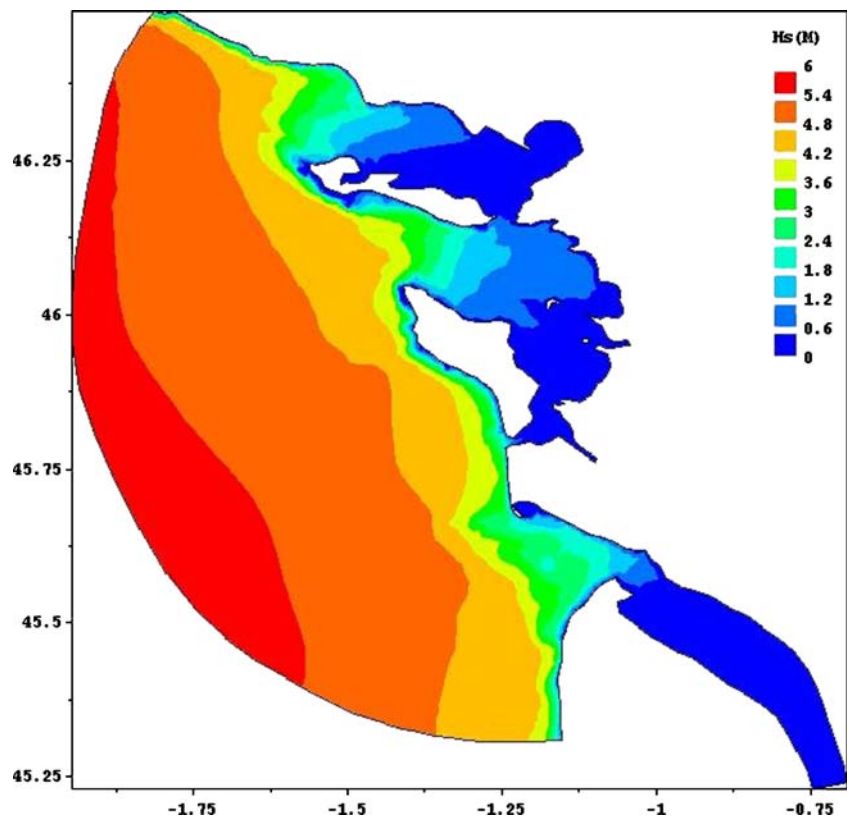
motion provoked by waves enhances the thickness of bottom boundary layer and modifies the mechanisms of energy dissipation by friction. The approach of Christoffersen and Jonsson (1985) used in this study is based on the turbulent viscosity models in evaluating the bottom stress. The total bed shear stress is divided into a sum of a bottom stress τ_{cb} induced by the currents and the bottom stress τ_{wb} due to waves:

$$\tau_b = \tau_{cb} + \tau_{wb} \tag{12}$$

The current component is related to the depth-averaged current velocity while the wave component is linked to the bottom orbital velocity of waves.

We refer the reader to Christoffersen and Jonsson (1985) for theoretical and computational details about the evaluation of the friction factors that relate the current velocity and the wave orbital velocity to the bed shear stress.

3.4.3 Radiation stress

Given the wave spectrum, $F(f,\theta)$, it is also possible to take into account the contribution of the wave motion to the mean flux of horizontal momentum described by the radiation stress tensor, S_{ij} (Longuet-Higgins and Stewart 1964) :

$$S_{ij} = \rho g \int_0^{2\pi} \int_0^{+\infty} \left[\frac{C_g}{C} \frac{k_i k_j}{k^2} + \left(\frac{C_g}{C} - \frac{1}{2} \right) \delta_{ij} \right] \times F(f,\theta) \mathrm{d}f \, \mathrm{d}\theta \tag{13}$$

where i and j point to the two horizontal coordinates x and y. δ_{ij} is the Kronecker symbol (=1 if $i=j$ and 0 elsewhere). An additional forcing term, $\mathbf{S_{rad}}$, is thus should be added to Eq. 2:

$$\mathbf{S_{rad}} = -\frac{1}{h\rho} \begin{pmatrix} \dfrac{\partial S_{xx}}{\partial x} + \dfrac{\partial S_{xy}}{\partial y} \\ \dfrac{\partial S_{yx}}{\partial x} + \dfrac{\partial S_{yy}}{\partial y} \end{pmatrix} \tag{14}$$

Following formula 13, the radiation stress is calculated by TOMAWAC and the forcing term 14 is then added to the right-hand side of Eq. 2 solved by TELEMAC 2D.

Fig. 8 The observed surge (*short dash*) versus that predicted by the large-scale model (*long dash*) and the local model (*solid line*) at La Pallice (**a**) and Chapus (**b**)
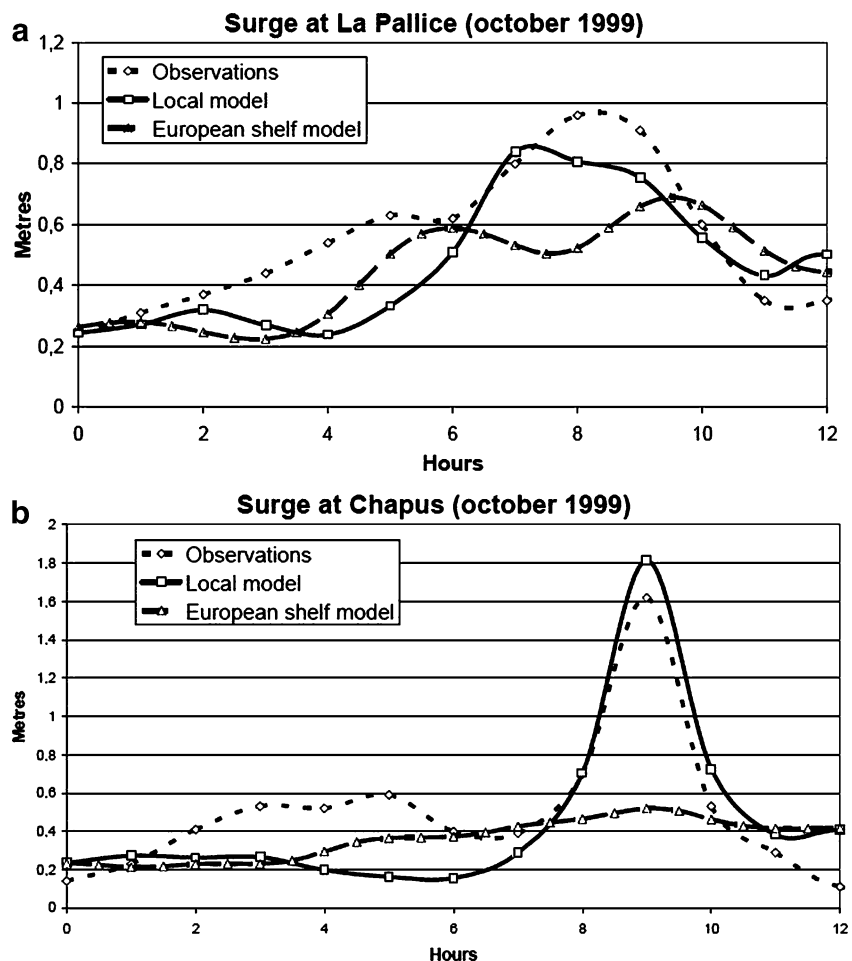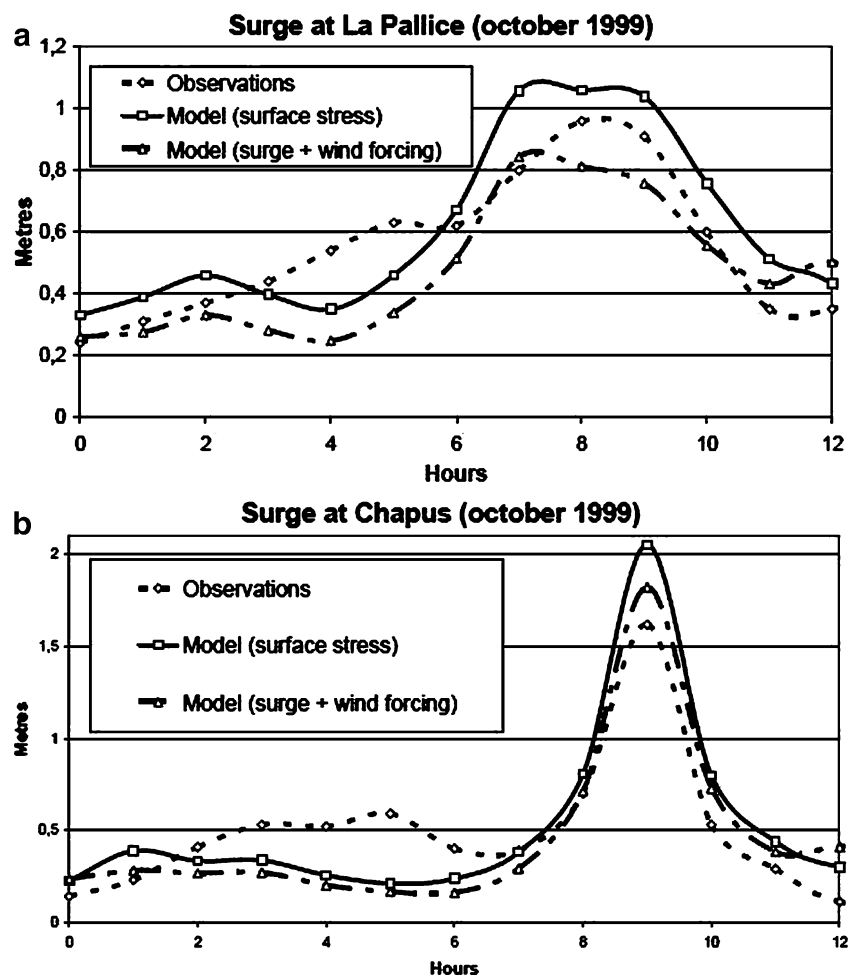
3.4.4 The coupling method

To take into account all the interactions between the different waves, we have applied the scheme displayed in Fig. 4. Sea state in the local model has been evaluated by running the TOMAWAC driven by wind (NOAA-CIRES) and by the wave spectrum estimated at the open boundary by the large-scale wave model (Fig. 3). The propagation of "tide + surge" in the local model is computed by the TELEMAC driven by (1) the tidal constituents at the open boundary given by the oceanic model of SHOM, (2) by the surge elevation provided by the oceanic model of Laboratoire National d'Hydraulique et Environnement (LNHE), (3) by the wind and pressure fields supplied by the meteorological model and (4) by the surface, bottom and radiation stresses provided by the local model of sea state.

4 Numerical simulations of the surge on 24 October 1999

To isolate the contribution on the surge dynamics due to various types of wave–wind–tide–surge interactions, we present in this section a set of the numerical experiments taking progressively into account the effect of model resolution, wave–wind coupling and bottom stress enhancement due to wave–current interactions as well as of the radiation stress. The results of simulations are compared with the observed surge elevations at tidal stations of La Pallice and Chapus.

4.1 The observed surge, the meteorological situation and the offshore waves

The storm surge has occurred during the night of 23–24 October 1999. It was generated by an atmospheric depression centred over Ireland before 23 October and moved southward from Ireland to the southern part of Bay of Biscay between 23 and 24 October. The speed and direction of the wind in the period 23–25 October are shown in Fig. 5. The wind speed has fluctuated from 12 to 18 m/s while its direction has been kept between approximately NW and NNW (Fig. 5).

The surges observed at two tidal stations in the Pertuis Charentais are displayed in Fig. 6. At La Pallice (station D in Fig. 1), the surge peak is recorded just after midnight, at 1 h (UT) on 24 October 1999 and at 3 h at Chapus (H in

Fig. 9 The observed surge (*short dash*) versus the freely propagating surge (*dot–dashed line*) and that with wind-induced surface stress (*continuous line*) at La Pallice (**a**) and Chapus (**b**)

Fig. 1). At these tidal stations, the surge height reached 1 and 1.6 m, respectively. The sea level uprising induced by the surge lasted about 4 h at Chapus where it had a pronounced bell-like shape. The surge at La Pallice was asymmetric and spread over 9 h. Note that the peak surge occurred during the spring tide, and the peak value at La Pallice corresponds to the tide 3 h before maximum flood.

A snapshot at the significant height, Hs, of the offshore waves 3 h before the surge peak at La Pallice is presented in Fig. 7. The Hs variations are typical during 6 h preceding the surge peak at La Pallice. The offshore waves are progressively damped towards the coast of the islands of Re and Oleron. Their height at the open western boundary of the model is about 6 m; it goes down to 4 m at the entrance to the Pertuis Charentais and then rapidly decreases, so that Hs is less than 1 m at La Pallice and less than 50 cm at Chapus. The offshore waves accompanying the 24 October surge were travelling from W to SW direction. Their peak period during the surge passage was very close to 10 s everywhere in the model domain.
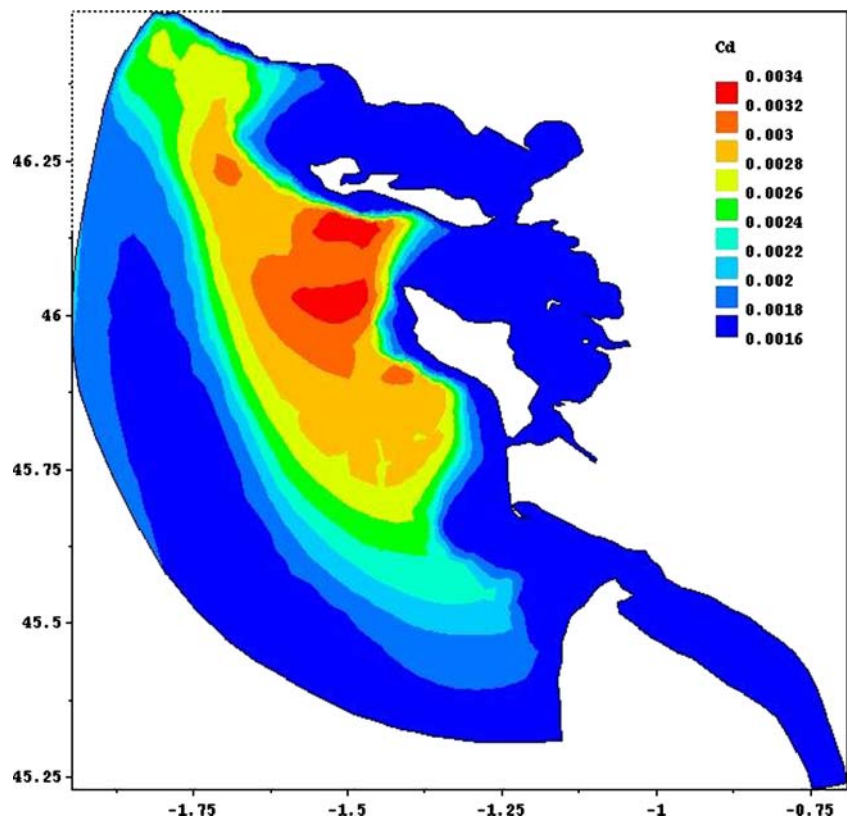
4.2 Freely propagating surge

First, we simulate a surge driven only by the sea level elevations imposed along the open offshore boundary as obtained from the large-scale LNHE model. Neither wind nor any of the wave–current interactions are taken into account, so that the sea surface in the local model is free of traction, and the bed friction is time independent. The amplitude of this freely propagating offshore surge is compared at La Pallice and at Chapus with the observed surge and with that predicted by the large-scale model in Fig. 8. A striking misfit between the observations and the large-scale model is due to its coarse grid unable to capture surge height variations and the peak surge. Employing a finer grid in the local model (Fig. 2) leads to a more realistic peak surge. The timing of the surge elevation peak is correctly reproduced at Chapus but is advanced by 2 h at La Pallice. Note that the shape of the predicted peak surge elevation at La Pallice is not as symmetric as that of the observed one.

It is interesting that, at La Pallice, the predicted surge peak is lower than the observed one by about 20 cm while it exceeds the observed surge at Chapus by approximately 20 cm. Contrary to La Pallice station, the tide gauge at Chapus is situated inside an area of extensive mud flats (Fig. 1) where seabed friction dominates inertial forces and leads to the specific diffusive propagation of tides and surges (Le Blond 1978; Parker 1984; Friedrichs and Madsen 1992). Consequently, the underestimation of surge peak at La Pallice and the overestimation of this at Chapus point to an increasing influence of seabed friction as tide and surges propagate into shallow near-shore regions of the Pertuis Charentais.

Fig. 10 The map of the surface drag coefficient at 22:00 h on 23 October 1999

4.3 Effect of the wind forcing

The observation that the freely propagating surge does not reach the observed peak amplitude at La Pallice (Fig. 8a) suggests that substantial surge amplification should be induced by the wind forcing. However, forcing the local model by the empirically computed wind traction (Eq. 5) turns out to be too weak to amplify significantly the freely propagating surge. The resulting surge is nearly indistinguishable from the freely propagating one and, by this reason, is not shown in Fig. 8. The weak influence of the wind on the peak surge is surprising, but it is, in fact, explained by spatial extension of the local model which is relatively small for the offshore surge could be affected noticeably by the surface drag created by the northeastern gale (Fig. 6) according to formula 5 (Nicolle 2006).

The wind effect is being strongly enhanced if the sea surface traction depends on the wave–wind interactions. In this case, the peak surge (Fig. 9) becomes higher than the freely propagating one by about 20 cm at La Pallice and by 50 cm at Chapus, and thus the predicted surge exceeds the observed one at both tidal gauges.

Some instructive insights on how the wind–wave coupling amplifies the surge are provided by a map of spatial variations of the sea surface drag coefficient C_d at 3 h before the peak surge elevation at La Pallice (Fig. 10). The surface drag rises up strongly along the western shores of the Island of Oleron and in the passage between the Island of Re and Island of Oleron where C_d becomes as large as 0.0033 which is significantly higher than the value of 0.0023 predicted by the empirical formula 5 for the same wind velocity. The largest magnitudes of C_d follow those of the wave-induced stress which is, in its turn, strongly enhanced on the near-shore shallow bottom (Fig. 1) where the offshore waves steepen, and their coupling with the atmosphere becomes stronger. As the waves advance into the Pertuis Charentais, they are effectively damped by friction (Fig. 7), and the interactions between waves and wind weaken rapidly.

The enhanced surface drag at the entrance to the Pertuis Charentais increases the wind-induced flux of the offshore water into both Pertuis as illustrated in Fig. 11, providing that the wind has a strong eastward component. This additional inflow of the offshore water is a physical cause

Fig. 11 The wind-induced water flux into the Pertuis Breton (**a**) and Pertuis d'Antioche (**b**). The *dashed line*: the surface drag is estimated by Smith and Banke formula (5); the *solid line*: by wind–wave–current interactions
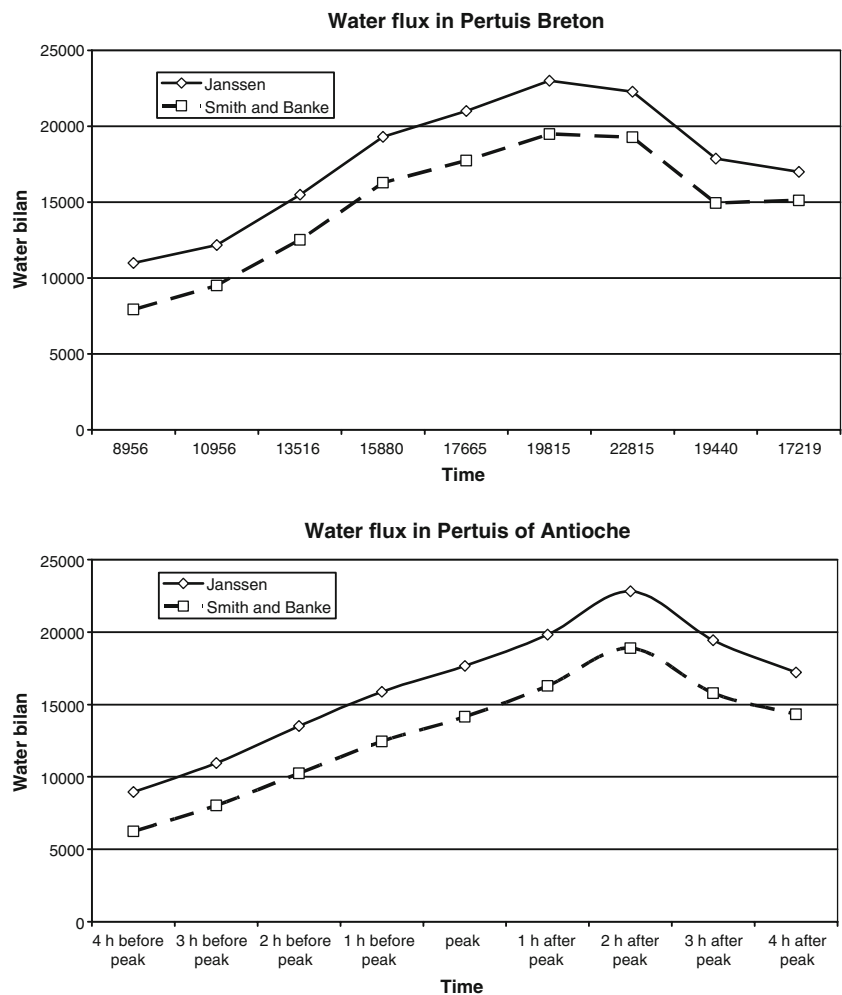
of the surge amplification by wave–wind interactions observed in Fig. 9. It is interesting to note that the maximum of the flow into both Pertuis Breton and Pertuis Antioche occurs 2–3 h later than the surge peak at La Pallice and coincides approximately with peak surge at Chapus.

4.4 Effect of the wave-dependent sea bottom friction

As demonstrated above, the enhanced wind–wave coupling without accounting for frictional interactions of waves with the seabed results in large overestimation of the surge elevations. In this section, the interaction of waves with currents at the seabed has been taken into account following Christoffersen and Jonsson (1985). Figure 12 compares the observations with the surges at La Pallice and at Chapus computed with and without the wave-dependent bottom friction. For both predicted surges, the wind–wave coupling is taken into account. As expected, the friction being enhanced by the wave–bottom interactions attenuates significantly the peak surges at both tidal stations. It is important, however, that inclusion of the wave-induced

friction makes the predicted surge peak value approach closer to the observed one. This bed stress enhancement induced by wave–current interaction results in decreasing the surge peak to the observed value at Chapus. The modelled surge peak is just 5 cm higher than that measured at La Pallice. Notice as well a more realistic bell-like shape of the peak surge shape at La Pallice when the wave bed friction is taken into account.

4.5 Influence of the radiation stress on the surge peak

Figure 13 presents the surge at La Pallice and at Chapus computed by taking into account the radiation stress. The additional surge rise provoked by the radiation stress is about 1–2 cm at both tidal stations. Similarly, a negligible influence of the radiation stress on the surge amplitude at La Pallice and Chapus has been estimated for other storm events (Nicolle 2006). This is explained by the strong attenuation of the waves propagating into the Pertuis Charentais (Fig. 2). The strong wave attenuation is due to strong bottom friction which damps effectively the swell waves. The computations made by Nicolle (2006) have

Fig. 12 The observed surge (*short dash*) versus the surges created by wind-induced surface stress without (*dot–dashed line*) and with (*solid line*) effect of waves on the bottom stress at La Pallice (**a**) and Chapus (**b**)
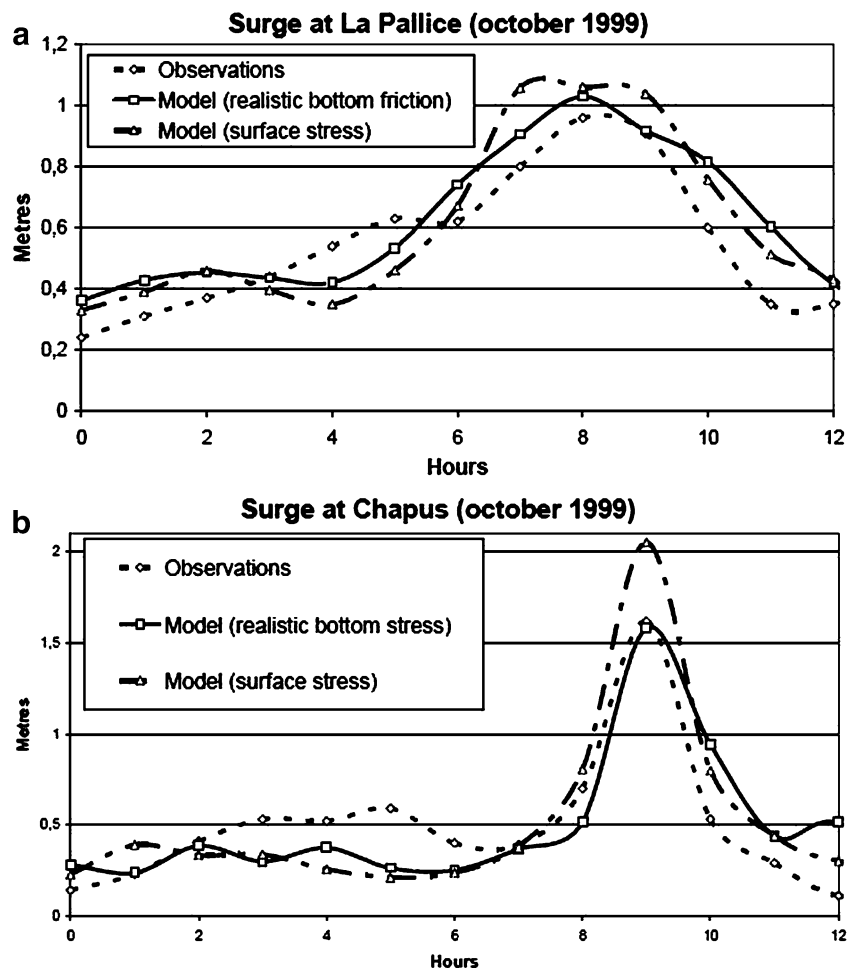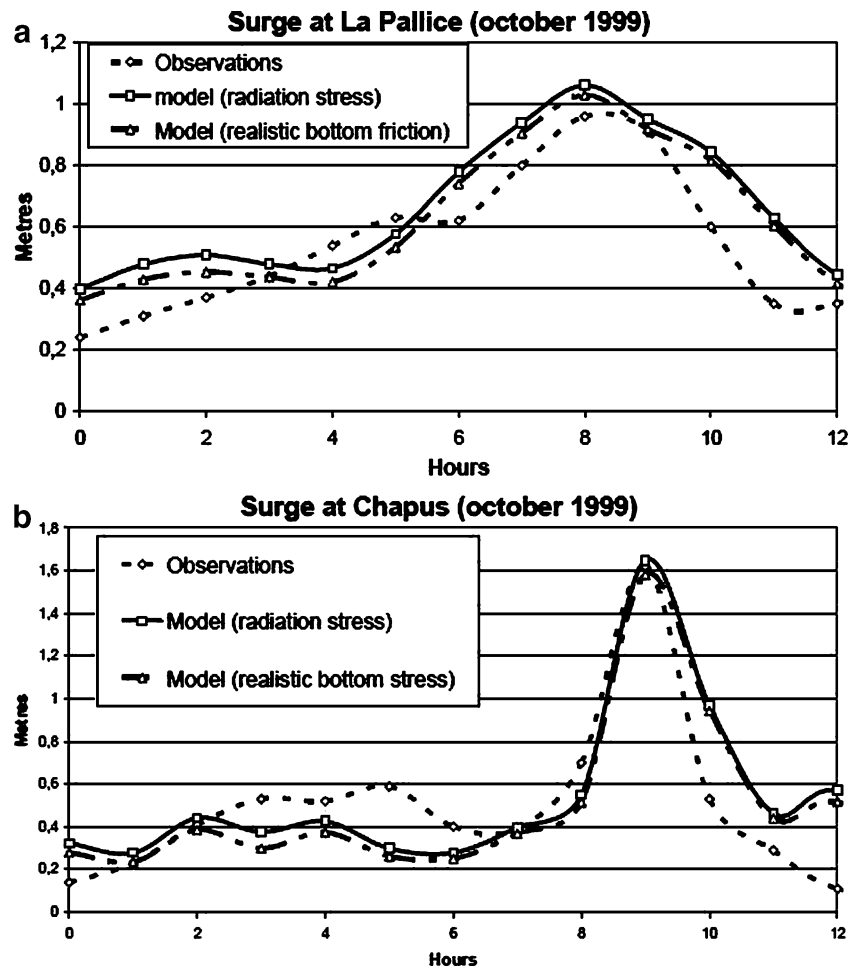
Fig. 13 The observed surge (*short dash*) versus the surges with (*solid line*) and without (*dot–dashed line*) taking into account the effect of radiation stress

shown that the radiation stress is more than an order of magnitude higher on the southwestern shores of the island of Oleron and on the western side of the island of Re than inside the Pertuis Charentais. Unfortunately, the lack of observations does not allow verifying these model predictions for the moment.

5 Summary and conclusions

A set of numerical simulations of the 24 October 1999 surge event has been carried out in order to evaluate the importance of the wind–wave–tide–surge interactions in the Pertuis Charentais. It turns out that the wind influence on the offshore surge is negligible when the wind-induced traction depends only on the wind speed as given by Smith and Banke formula. On the other hand, the surge peak is amplified by nearly 20% in a model incorporating the wave–wind–current interactions following Janssen (1991) approach.

The enhancement of the storm surge observed in numerical experiments is a local effect in the sense that it is entirely due to the interactions of the waves with the

complex coastal geometry and shallow sea bottom at the entrance to the Pertuis Charentais. The steepening of the waves at the entrance to the Pertuis Charentais has led to a locally increased sea surface roughness that has enhanced the effective drag coefficient at the surface (Fig. 10). Consequently, the northwesterly wind has increased the flux of the offshore water into the Pertuis Charentais and has amplified the external offshore surge. It is worthy of note that the intensity of the surface drag enhancement is rather sensitive to the direction and amplitude of the waves and those of the wind in respect to the western shores of the Pertuis Charentais.

The results obtained in this study confirm the findings of Mastenbroek et al. (1993) and Brown and Wolf (2009) who have demonstrated a significant effect of young waves on the storm surge amplification through the sea surface drag enhancement in the Northern Sea and in the Irish Sea, respectively. This sensitivity of the surface drag enhancement to the wave age and, more generally, on sea state means that any modelling system aimed at flood forecasting in a region where the wave age varies significantly should take into account the impact of the wave–tide–surge coupling on surge propagation.

References

Benoit M (2003) Logiciel TOMAWAC de modélisation des états de mer en éléments finis. Notice théorique de la version 5.2. Note technique EDF R&D LNH HP-72/02/065/A

Benoit M, Marcos F, Becq F (1996) Development of a third generation shallow water wave model with unstructured spatial meshing. In: Proc. 25th Int. Conf. on Coastal Eng. (ICCE'1996), 2–6 Septembre 1996, Orlando (Florida, USA), pp 465–478

Benoit M, Marcos F, Janin JM (1997) Interactions atmosphère/houle/marée/surcotes appliquées à la simulation des tempêtes en mer. In: Proc. Symp. Saint-Venant "Analyse Multiéchelle et systèmes physiques couplés", 28–29 August 1997, Paris (France), pp 211–218 (in French)

Bernier NB, Thompson KR (2007) Tide-surge interaction off the east coast of Canda and northeastern United States. J Geophys Res v112, C06008. doi:10.1029/2006JC003793

Bowden KF, Krauel DP, Lewis RE (1974) Some features of turbulent diffusion from a continuous source at sea. Adv Geophys 18A:315–329

Brown J, Wolf J (2009) Coupled wave and surge modeling for the eastern Irish Sea and implications for model wind-stress. Cont Shelf Res 29:1329–1342

Carretero Albiach JC, Álvarez Fanjul E, Gómez Lahoz M, Pérez Gómez B, Rodríguez Sánchez-Arevalo I (2000) Ocean forecasting in narrow shelf seas: application to the Spanish coasts. Coastal Eng 41:269–293

Christoffersen JB, Jonsson IG (1985) Bed friction and dissipation in a combined current and wave motion. Ocean Eng 12(5):387–423

Davies AM, Lawrence J (1995) Modelling the effect of wave–current interaction on the three-dimensional wind-driven circulation of the Eastern Irish Sea. J Phys Oceanogr 25:29–45

Ezer T, Mellor GL (2000) Sensitivity studies with the North Atlantic sigma coordinate Princeton Ocean Model. Dyn Atmos Ocean 32 (3/4):185–208

Flather RA (2000) Existing operational oceanography. Coastal Eng 41:13–40

Friedrichs CT, Madsen OS (1992) Nonlinear diffusion of the tidal signal in frictionally dominated embayments. J Geophys Res 97 (C4):5637–5650

Heaps NS (1965) Storm surges on a continental shelf. Philos Trans R Soc London Ser A 257:351–383

Hervouet J-M (2007) Hydrodynamics of free surface flows, modelling with the finite element method. Wiley, Hoboken. ISBN 978-0-470-03558

Hervouet JM, Van Haren L (1994) Système de modélisation TELEMAC: TELEMAC-2D note de principe. LNHE de l'EDF (in French)

Idier D, Pedreros R, Oliveros C, Sottolichio A, Choppin L, Bertin X (2006) Contributions respectives des courants et de la houle dans la mobilite sedimentaire d'une plate-forme interne estuarienne. Exemple: le seuil interinsulaire, au large du Pertuis d'Antioche, France, Comptes Rendus. Geoscience 338:718–726

Janssen PAEM (1991) Quasi-linear theory of wind–wave generation applied to wave forecasting. J Phys Oceanogr 19:745–754

Jones JE, Davies AM (1998) Storm surge computations for the Irish Sea using a three-dimensional numerical model including wave–current interaction. Cont Shelf Res 18:201–251

JONSWAP Group (1973) Measurements of wind-wave growth and swell decay during the Joint North Sea Wave Project. Dtsch Hydrogr Z A8:95

Le Blond PH (1978) On tidal propagation in shallow rivers. J Geophys Res 83:4717–4721

Le Roy R, Simon B (2003) Réalisation et validation d'un modèle de marée en Manche et dans le Golfe de Gascogne. SHOM Rapport d'étude no. 002/03

Longuet-Higgins MS, Stewart RW (1964) Radiation stresses in water waves; a physical discussion, with application. Deep-Sea Res 11:526–562

Luettich RA Jr., Westerink JJ, Scheffner NW (1992) ADCIRC: an advanced three-dimensional circulation model for shelves, coasts, and estuaries. Technical Report DRP-92-6, US Army Engineer Waterways Experiment Station, Vicksburg

Mastenbroek C, Burgers G, Janssen PAEM (1993) The dynamical coupling of a wave model and a storm surge model through the atmospheric boundary layer. J Phys Oceanogr 23:1856–1866

Nicolle A (2006) Modélisation des marées et des surcotes dans les Pertuis Charentais (Golfe de Gascogne), Ph.D. thesis, Université de La Rochelle, 307 pp

Nicolle A, Karpytchev M (2007) Evidence for spatially variable friction from tidal amplification and asymmetry in the Pertuis Breton (France). Cont Shelf Res 27:2346–2356

Parker B (1984) Frictional effects on the tidal dynamics of a shallow estuary. Ph.D. Thesis, John Opkins University, Baltimore, 292 pp

Proudman J (1953) Dynamical oceanography. Methuen, London 409 pp

Smith SD, Banke EG (1975) Variation of the sea surface drag coefficient with wind speed. Q J R Meteor Soc 101:665–673

Williams JA, Flather RA (2000) Interfacing the operational storm surge model to a new mesoscale atmospheric model. POL Internal Document, No. 127, Proudman OceanographicLab., Liverpool, 18 pp

Wolf J, Hubbert KP, Flather RA (1988) A feasible study for the development of a joint surge and wave model. Proudman Oceanographic Laboratory, Rep. N1

Wolf J (2009) Coastal flooding—impacts of coupled wave–surge–tide models. Natural Hazards v.9:241–260

Xie L, Pietrafesa LJ, Wu K (2003) A numerical study of wave–current interaction through surface and bottom stresses: coastal ocean response to Hurricane Fran of 1996. J Geophys Res 108 (2):3049